Molecular Endocrinology. First published January 9, 2003 as doi:10.1210/me.2002-0290

Gene expression profiling reveals progesterone-mediated cell cycle and immunoregulatory roles of *Hoxa-10* in the pre-implantation uterus

Mylene W. M. Yao [1,2,#], Hyunjung Lim[3], Daniel J. Schust[2], Sung E. Choe[1,4], Anna Farago[1], Yueyun Ding[1], Sebastien Michaud[1], George M. Church[4] and Richard L. Maas[1*]

[1] Division of Genetics, Department of Medicine, Brigham and Women's Hospital and Harvard Medical School, Boston, MA 02115

[2] Department of Obstetrics and Gynecology, Brigham and Women's Hospital, Harvard Medical School, Boston, MA 02115

[3] Departments of Obstetrics and Gynecology, and Cell Biology and Physiology, Washington University School of Medicine, St. Louis, MO 63110

[4] Department of Genetics, Harvard Medical School, Boston, MA 02115

* Corresponding author: Richard L. Maas, M.D., Ph.D., tel. 617-732-5856; fax 617-732-5123; *e-mail:* maas@rascal.med.harvard.edu

Present Address: Department of Obstetrics and Gynecology, Columbia University College of Physicians and Surgeons, New York, NY 10032

Running Title: Expression profile in the *Hoxa-10* mutant uterus

Keywords: progesterone, uterine stroma, implantation, *Hoxa-10*, gene expression profiling, cell cycle, proliferation, p15, p57, BrdU, T lymphocytes, *Hoxa-11*, cross-regulation

Abstract

Human infertility and recurrent pregnancy loss caused by implantation defects are poorly understood. *Hoxa-10* deficient female mice have severe infertility and recurrent pregnancy loss due to defective uterine implantation. Gene expression profiling experiments reveal that *Hoxa-10* is an important regulator of two critical events in implantation – stromal cell proliferation and local immunosuppression. At the time of implantation, *Hoxa-10* mediates the progesterone stimulated proliferation of uterine stromal cells. *Hoxa-10* mutants express a stromal cell proliferation defect that is accompanied by quantitative or spatial alterations in the expression of two cyclin dependent kinase inhibitor (CKI) genes, *p57* and *p15*. *Hoxa-10* deficiency also leads to a severe local immunologic disturbance, characterized by a polyclonal proliferation of T cells, that occurs in place of the normal progesterone-mediated immunosuppression in the peri-implantation uterus.

Introduction

Infertility affects more than 6.1 million women and their partners in the U.S. Implantation failure due to intrinsic uterine defects is thought to span a wide clinical spectrum including spontaneous abortion, unexplained infertility and recurrent pregnancy loss (1). Gene targeting in mouse models has identified several genes that are critical for implantation (reviewed in 2, 3). A complex series of synchronized molecular interactions occur within the uterus prior to implantation, and between the uterus and the implanting blastocyst, both of which are required for successful implantation.

At the same time, gene targeting studies show that implantation of a healthy embryo can fail due to a defective uterine environment. Priming of the uterine stroma by progesterone is

essential for the establishment of an appropriate uterine environment for implantation. Although knowledge of the molecular pathways that act downstream of progesterone (P4) in implantation is limited, one gene that is both P4-responsive and required for the establishment of an appropriate environment for embryo implantation in the mouse uterus is *Hoxa-10*, a member of the *AbdB* subclass of *Hox* genes (4-6). Although *Hox* genes are well known as regulators of patterning in both vertebrate and invertebrate embryonic development, *Hoxa-10* deficient adult female mice exhibit a severe failure of implantation and defective decidualization that lead to recurrent pregnancy loss and infertility (6).

The uterus is comprised of three major cellular compartments – epithelium, stroma, and myometrium, which are under differential hormonal regulation by ovarian estrogens and progesterone (2, 3). In murine reproductive physiology, the major pre-ovulatory ovarian estrogen, estradiol, stimulates the uterine epithelium on day 0.5 to 1.5 post coitum (p.c.), while P4 stimulation of the uterine stroma is first evident by day 2.5 p.c. On day 3.5 p.c., estrogen levels rise again so that the uterine stroma has been sequentially primed by estrogen and progesterone and is now regulated by both hormones simultaneously (2).

Hoxa-10 is upregulated by P4 in the uterine stroma at day 3.5 p.c., 24 hours prior to implantation, and its expression persists in the developing decidua (5, 7). Moreover, previous studies have shown that *Hoxa-10* is required for P4 responsiveness in the uterine stroma (8). For example, in a model in which *Hoxa-10* mutant females are ovariectomized to eliminate variability in hormonal cycling between animals, then treated with estrogen and progesterone, stromal cell proliferation is impaired, while epithelial cell proliferation is unaffected. In this assay, exogenous progesterone and estrogen greatly amplify the magnitude of the basal uterine stromal proliferation defect in ovariectomized *Hoxa-10* mutants relative to wild type (8).

Hox genes have been proposed to act as local regulators of cell proliferation during development (9, 10), but molecular effectors for their proposed cell cycle regulatory function have not been identified. Based on the observed proliferation defect in the *Hoxa-10* mutant stroma, we reasoned that P4 administration to ovariectomized wild type and *Hoxa-10* deficient females should amplify differences in gene expression that underlie the *Hoxa-10* mutant stromal proliferation defect. We therefore employed global gene expression profiling to identify *Hoxa-10* downstream genes that mediate the stimulatory effect of P4 on cell cycle progression in the uterine stroma. At the same time, we sought to gain insight into other P4-dependent downstream events that contribute to the defective implantation phenotype in *Hoxa-10* mutant females.

While implantation depends upon the precisely coordinated effects of estrogen and progesterone, in order to study the effects of one steroid hormone at a time, we initially chose to focus only on the gene expression changes produced by progesterone. However, in order to establish physiologic relevance of findings derived from an ovariectomy model to normal implantation, we then further evaluated the results in a combined E2+P4 context, day 3.5 p.c. of natural pregnancy.

RESULTS

Experimental design: general considerations

To identify genes that are differentially expressed between wild type and *Hoxa-10* mutants, RNA was collected from uteri of ovariectomized female mice 6 hours after P4 injection (Fig. 1A). In the ovariectomy model, denoted OVX/P4/6h, in which ovarian production of endogenous progesterone and estradiol is absent, P4 injection permits the study of differential gene expression specific to the mediation of the progesterone response by *Hoxa-10*. To extend the

previous finding that *Hoxa-10* mRNA expression is significantly upregulated in the uterine stroma 6 hours after P4 injection (6), we performed Western blot analyses for Hoxa-10 protein expression at 0, 1, 3, 6, 9, 12, 18 and 24 hours after P4 injection. Hoxa-10 protein was upregulated in response to P4 and reached its peak expression 6 hours after injection (Fig. 1B). Hoxa-10 protein levels are stable at the later time points, declining by 24 hours (data not shown). The 6 hour timepoint was therefore chosen to optimize the identification of immediate or near-immediate targets of *Hoxa-10*. Compared to the physiologic peri-implantation uterus, the proportion of stroma to epithelium is greater in the OVX/P4/6h model. Thus, the strategy chosen was designed to maximize the yield of *Hoxa-10* downstream genes in the uterine stroma.

Since we sought to study the function of *Hoxa-10* in the pre-implantation uterus, we then further tested the *in vivo* relevance of select candidate downstream genes derived from the OVX/P4/6h model in the context of normal pregnancy. This was done in day 3.5 p.c. pregnant mice by using quantitative real time RT-PCR, *in situ* hybridization, flow cytometry and BrdU incorporation experiments (Fig. 1A). We chose day 3.5 p.c. as it represents an early physiologic time point in the response of the uterus to P4 and coincides with the onset of *Hoxa-10* expression in the uterine stroma. Furthermore, it precedes the earliest observable implantation defect, the failure of embryo attachment to the uterus, which normally occurs late on day 3 p.c. Therefore, to a first approximation, differential gene expression occurring at day 3.5 p.c. is less likely to reflect a failure of implantation and more likely to reflect changes in gene expression that contribute to the implantation defect in the *Hoxa-10* mutant.

Gene expression profiling detects differentially regulated genes (DRGs) in the *Hoxa-10* mutant uterine stroma

Gene expression profiles of more than 12,000 genes (6000 known genes and 6000 ESTs) represented on the U74Av.2 oligonucleotide array (Affymetrix, Santa Clara, CA) were first analysed by dChip (11, 12). All subsequent analyses were performed on dChip model-based expression indices. The fold difference cutoff in all analyses was 1.5-fold unless otherwise specified. Independent analyses using Statistical Analysis of Microarrays (SAM) and conventional t test (13, 14) yielded 92 and 81 genes, respectively, that were differentially expressed between wild type and *Hoxa-10* mutant uteri in the OVX/6h/P4 model (Table 1A). A total of 57 genes were identified by both SAM and t test. The high degree of overlap (>50%) between these two analytical methods, which are based on very different statistical assumptions, points to the robustness of the data analysis. Combining the gene lists obtained by SAM and t test yielded a total of 116 differentially regulated genes, or DRGs, and all subsequent data analyses and experiments were based on these 116 DRGs (Table 1A).

Of the 116 DRGs, 26 genes were more highly expressed in the wild type uterus, while 90 genes were more highly expressed in the *Hoxa-10* mutant uterus (Tables 1B, C; 15, 16; see Web Supplement for complete list of data and their corresponding GEO accession numbers, 12). The preponderance of upregulated DRGs in the *Hoxa-10* mutant uterus in response to P4 was robust and pertained regardless of the threshold fold difference. This result suggests that the predominant downstream effect of *Hoxa-10* in this tissue is repressive, or that *Hoxa-10* upregulates transcriptional repressors. None of the DRGs were significantly differentially regulated in control experiments in which oil vehicle rather than P4 was injected (data not

shown; 15, 17). The functional categories represented by the DRGs and the number of DRGs in each category are listed in Table 2. The five predominant functional categories of DRGs relate to: (1) immune, complement and chemokine functions; (2) enzyme function or metabolism; (3) adipocyte function, fat metabolism and energy balance; (4) transcriptional regulation; and (5) cell cycle control and cell proliferation. A panel of eight DRGs representing different functional categories was quantitatively validated by real time RT-PCR. Consistent with the microarray data, *Hoxa-11*, *Follistatin* and *Slap* were more highly expressed in wild type relative to *Hoxa-10* mutant uterus, while *Adipsin*, *Inhibitor of DNA binding–1*, *Lactotransferrin*, *Gas6* and *p57* were more highly expressed in the *Hoxa-10* mutant (12). In addition, the stromal expression of 14 DRGs, including five of the above-mentioned genes, was either demonstrated by *in situ* hybridization experiments or ascertained from the literature (12). Thus, the experimental strategy was successful in enriching for stromally expressed *Hoxa-10* dependent DRGs in the pre-implantation uterus.

Hoxa-11 **is co-regulated by** ***Hoxa-10*** **and P4**

As *Hoxa-11* is known to be up-regulated by P4 (7), we independently analyzed all RNA samples by real-time RT-PCR analysis for *Hoxa-11* expression to determine whether its expression is altered in the *Hoxa-10* mutant uterus. Compared to wild type mice injected with oil, mice injected with P4 showed significantly higher *Hoxa-11* expression levels at each time point analyzed, with peak expression occurring at 6 hours (Fig. 2A). Notably, however, the induction of *Hoxa-11* expression was markedly attenuated in *Hoxa-10* mutant uteri compared to wild type. In four independent real time RT-PCR experiments, each conducted in triplicate and consisting of pooled uterine RNA from 4 wild type and 4 mutant mice, the mean normalized *Hoxa-11*

expression level was 2.5 ± 0.2 (mean ± SEM) in wild type, compared to 1.5 ± 0.1 in *Hoxa-10* mutants (Fig. 2B). This attenuation in *Hoxa-11* expression in the *Hoxa-10* mutant 6 hours after P4 injection was highly significant ($p = 0.01$; 2-tailed t test). Therefore, as suggested by the microarray analysis (Table 1B) and confirmed by real time RT-PCR, the uterine stromal expression of *Hoxa-11* is positively regulated, directly or indirectly, by *Hoxa-10* as well as by P4.

Identification of additional genes that are co-regulated by *Hoxa-10* and P4

We next tested the DRGs for further evidence of co-regulation by using a time series model, in which uteri were collected from ovariectomized wild type mice at 0, 1, 3, 6, 9, 12, 15, 18 and 24 hours after P4 injection (15, 18). In contrast to the OVX/P4/6h model in which genotype (wild type vs. mutant) was the variable, in the time series model, genotype was constant (wild type only) while the time after P4 injection exposure varied. A self-organizing map (SOM) algorithm (19) was used to cluster genes that showed sufficient variation in expression during the time series. The criteria for "sufficient variation" were: (1) the minimum fold change in expression level between at least two time points is greater than 2; and (2) the minimum difference in expression level between at least two time points is greater than 75 units. 1675 genes fulfilled the inclusion criteria and were grouped into 18 clusters. The SOM algorithm arranged the clusters as nodes in a 3×6 grid configuration, with the physical distance between two clusters on the grid reflecting the degree of similarity of their expression profiles. As a result, adjacent clusters are more similar than non-adjacent clusters. The 3×6 arrangement of these 18 SOM clusters and their respective gene lists can be viewed in the Web Supplement (12).

Four such clusters are shown in Figure 3. Cluster 3 demonstrates the consistency of the data and the power of this analytical method in clustering co-regulated genes. 78% (40/51) of the genes in Cluster 3 consisted of immunoglobulin (*Ig*) genes, which are B lymphocyte specific (Fig. 3A). Interestingly, there was no apparent difference in the regulation of these *Ig* genes between wild type and mutant. Nonetheless, the striking coordinate down-regulation of *Ig* genes in response to P4 indicates that major changes in the dynamics of intra-uterine B cell trafficking, *Ig* gene expression, or both, occur in response to P4.

Of the 18 time series SOM clusters, 3 contain a significantly large number of DRGs, based on calculations using a hypergeometric distribution, followed by Bonferroni correction for multiple tests (Table 3, Fig. 3B, 12, and 20). Clusters 1, 5, and 6 are significantly enriched with 12, 7 and 15 DRGs, respectively, ($p<0.003$; Fig. 3B). The p-values calculated for the enrichment of each cluster are listed in Table 3. Interestingly, while Cluster 3 consists predominantly of genes of the *Ig* family, Clusters 1, 5 and 6 contain genes with diverse functions. The enrichment of DRGs in clusters derived from the P4 time series model reflects their co-regulation by Hoxa-10 and P4 and further supports the premise that the DRGs identified in the OVX/P4/6h model are relevant to implantation.

Hoxa-10 alters expression of the CKI genes *p57(Kip2)* and *p15(Ink4b)*

To further evaluate the *in vivo* relevance of DRGs identified in the OVX/P4/6h model, we tested specific DRGs for their differential regulation in wild type and *Hoxa-10* mutant uteri at day 3.5 p.c. of pregnancy. Interestingly, the expression of two cyclin dependent kinase inhibitor (CKI) genes, *p57(Kip2)* and *p15(Ink4b)* was altered, either quantitatively or qualitatively, in the day 3.5 p.c. *Hoxa-10* mutant uterus. While in situ hybridization revealed that *p57* was diffusely

expressed throughout both day 3.5 wild type and mutant stroma (data not shown), quantitative real time RT-PCR indicated that *p57* transcripts were increased by 6.6 ± 1.8 fold (mean ± SEM; $p<0.08$) in the mutant (Fig. 4A), consistent with microarray results of the OVX/P4/6h model.

On the other hand, although microarray analysis suggested that *p15* expression in the OVX/P4/6h model was decreased in the mutant, this result was not confirmed by real time RT-PCR analysis of day 3.5 p.c. uterine RNA. Instead, these analyses showed only a non-significant increase in *p15* expression in mutant relative to wild type (Fig. 4A). Nonetheless, to our surprise, in situ hybridization showed that the spatial expression pattern of *p15* was clearly altered in the *Hoxa-10* mutant at day 3.5 p.c. (Fig. 4B). In contrast to the restricted wild type expression of *p15* in the submyometrial stroma and myometrium, in the *Hoxa-10* mutant uterus, *p15* was expressed throughout the entire stroma (Fig. 4B). Similar results were observed in the OVX/P4/6h model (data not shown). Collectively, these results provide a link between *Hox* gene function and the expression of cell cycle regulatory genes, and provide a potential molecular correlate to the cell proliferation defect previously observed in the *Hoxa-10* ovariectomy model following combined E2 plus P4 treatment (8).

Uterine stromal cell proliferation is inhibited in *Hoxa-10* mutants

To test whether stromal cell proliferation was disrupted on day 3.5 p.c. of natural pregnancy in the *Hoxa-10* mutant uterus, we injected day 3.5 p.c. pregnant wild type and mutant mice with BrdU, and 4 hours later, performed immunostaining on freshly isolated uterine stromal cells with anti-BrdU antibody. The immunostained cells were then analyzed by flow cytometry. In wild type mice, 8.9% ± 0.1% (mean ± SEM) of uterine stromal cells were $BrdU^+$, with 5% background fluorescence in unstained control cells. However, in 4 replicate experiments in the

Hoxa-10 mutant, only 5.7 ± 0.2% of uterine stromal cells were $BrdU^+$ (Fig. 4C). The decrease in the proportion of stromal cells that incorporated BrdU in the *Hoxa-10* mutant was significantly lower than in wild type ($p < 0.01$). The decrease in S-phase entry by mutant uterine stromal cells indicates an important cell cycle regulatory function of *Hoxa-10* that is compatible with the altered expression of *p57* and *p15* in the *Hoxa-10* mutant peri-implantation uterus.

Expression profiling detects abnormal accumulation of T lymphocytes in the *Hoxa-10* mutant uterus

We next investigated the biological relevance of a second group of DRGs that was expressed at higher levels in the *Hoxa-10* mutant uterus than in wild type: those pertinent to immune function. In particular, genes expressed in T lymphocytes, including *TCRγV4, TCRδC* and *MHC class II I-A^b*, were over-expressed in the *Hoxa-10* mutant uterine expression profile. While this result could reflect increased expression of these genes on a per cell basis, we first chose to test the hypothesis that T lymphocytes, a distinct cell population in the uterine stroma, were increased in number in the *Hoxa-10* mutant. Indeed, flow cytometry of cells isolated from the uterine stroma of day 2.5 and 3.5 p.c. pregnant mice, with splenocytes as a control, indicated that the proportions of $CD4^+$ and $CD8^+$ T cells were significantly increased in the mutant uterine stroma (Fig. 5A). In addition, this expansion of T cells was polyclonal, as evident by increases in TCRγδ, TCRαβ and NK lineages in the *Hoxa-10* mutant uterus on day 3.5 p.c. (Fig. 5A, 5B). Consistent with microarray results showing increased expression of *TCRγV4* and *TCRδC* in the *Hoxa-10* mutant, the increase in the number of γδ T cells in the physiologic pregnant state occurred earliest and was the most dramatic (Fig. 5A). Microarray analysis of heterogeneous uterine tissue thus revealed alterations in gene expression that at least partly reflected changes in

cell number within specific stromal T cell subpopulations. These analyses thus indicate a significant and previously unsuspected immunological phenotype in the *Hoxa-10* mutant uterus.

Hyper-proliferation of T lymphocytes in the *Hoxa-10* mutant uterine stroma

Alterations in lymphocyte proliferation, trafficking, or both could underlie the increased number of T cells present in the *Hoxa-10* mutant uterus. To test the first possibility, we performed BrdU labeling followed by flow cytometry of uterine lymphocyte populations. These analyses showed an increased proliferation of T cells in the mutant uterine stroma. Thus, even though the overall proliferation index of cells present in day 3.5 p.c. mutant uterine stroma was decreased (Fig. 4C), the proportions of double positive $CD4^+BrdU^+$ and $TCR\gamma\delta^+BrdU^+$ cells were actually higher in the mutant uteri by 5.3 ± 2.5 and 1.8 ± 0.1 (mean ± SEM) fold, respectively (data not shown). These results were derived from two separate experiments, each of which comprised pooled day 3.5 p.c. uteri from 5 mutant and 5 wild type mice. One experiment was performed after a syngeneic mating, while the second experiment was performed after an allogeneic mating; both experiments gave similar results. The disparity between the proliferation rate of cells in the uterine stroma, analyzed *en masse*, which is depressed in the *Hoxa-10* mutant, and the proliferation rates of specific intrauterine T lymphocyte subpopulations, which are increased in the *Hoxa-10* mutant, highlights the dynamic nature of the uterine environment at the time of implantation.

We performed immunostaining experiments to further confirm the localization of T cells in the uterus. We chose the CD4 marker for these localization experiments as $CD4^+$ cells were twice as abundant as $CD8^+$ cells in all flow cytometry experiments, as seen in the representative experiment in Fig. 5B. Immunostaining experiments confirmed that the $CD4^+$ cell population

resided mainly in the stromal compartment in both wild type and *Hoxa-10* mutant uterus at both days 0.5 and 3.5 p.c. (Fig. 5C). On day 0.5 p.c., when estrogen effects predominate, there was no overt difference in $CD4^+$ abundance between wild type and *Hoxa-10* mutant uterus. At day 3.5 p.c., however, when P4 levels are high, $CD4^+$ immunostaining was greater in the mutant stroma than in wild type (Fig. 5C). The day 3.5 $CD4^+$ immunostaining results are thus consistent with the $CD4^+$ flow cytometry analyses (Fig. 5A).

Discussion

Fidelity of expression profiling applied to mouse implantation

We have demonstrated that gene expression profiling can be used to analyze the hormonal control of implantation by employing a gene-targeted mouse model to dissect the pre-implantation events downstream of *Hoxa-10*. A key feature of this approach was the experimental design, which proved crucial for identifying the enrichment of *Hoxa-10* dependent DRGs expressed in the P4-primed uterine stroma. In addition, comparison of experimental data obtained under conditions of varied genotype and duration of P4 exposure permitted the identification of subsets of genes that are likely to be co-regulated by *Hoxa-10* and by P4.

An attenuation of P4-induced *Hoxa-11* expression was identified in the *Hoxa-10* mutant uterus by both microarray and real time RT-PCR. This result was previously not identified by in situ hybridization (8), likely because of the inherently non-quantitative nature of this technique. Cross-regulation of *Hox* genes in embryonic patterning is well known (21), as exemplified by the regulation of *Hoxb2* by *Hoxb1* in rhombomere r4 during mouse embryonic development (22). The cross-regulation of *Hoxa-11* by *Hoxa-10* also has important implications in implantation, including the possibility that the PR and Hoxa-10 functionally cooperate to mediate the full

induction of *Hoxa-11* stromal expression. The relevance of *Hoxa-10* and *Hoxa-11* regulatory interactions to the study of human infertility is further supported by the finding of up-regulated *HOXA-10* and *HOXA-11* expression in the human uterus in response to P4 during the time of implantation (23).

Comparison to other microarray studies

The experimental approach described here differs from that in other microarray studies designed to identify genes involved in implantation (24-26). In one study, the same Affymetrix microarray (U74A ver. 2) used in our analyses was used to identify genes that are differentially expressed between implantation and non-implantation sites in the wild type uterus at 23-24 hours of day 3 p.c. (26). In our study, we employed unopposed P4 stimulation in wild type and *Hoxa-10* mutant females to identify *Hoxa-10* dependent DRGs in the uterine stroma. Under these conditions, *Hoxa-10* expression is strongly induced throughout the uterine stroma (7), a situation that should favor the identification of P4 inducible *Hoxa-10* dependent stromal target genes. Importantly, however, we also tested the *in vivo* relevance of these DRGs in a physiologic pregnancy model at a timepoint, the morning of day 3 p.c., before implantation and non-implantation sites are distinguishable. This strategy thus permitted validation of the findings from the OVX/P4/6h model, and should have enriched for *Hoxa-10*-regulated events that precede overt morphological signs of implantation failure in the mutant.

Thus, while our OVX/P4/6h model cannot be directly compared to the above-mentioned study, data from our OVX/P4/18h experiments (data not shown), in which uterine RNA was extracted at 18 hours after P4 injection, does detect some of the same DRGs reported by Reese et al. (26). For example, *BiP*, encoding a calcium-binding Hsp70 class chaperone

(reviewed in ref. 27), is expressed at higher levels in the wild type than in the *Hoxa-10* mutant uterus. The same gene was also found by Reese et al. to be more highly expressed in wild type implantation sites than inter-implantation sites (26). The expression of genes such as *BiP* may thus mark a later time point in the P4 response than that addressed by the OVX/P4/6h model.

An especially interesting point of similarity between the present data and that of Reese et al. (26) relates to the striking, coordinate regulation of some 41 *Ig* genes in cluster 3 of our SOM analysis. These transcripts are markedly reduced by 3 hours after P4 injection, followed by a small peak of expression at 6 hours and a slow return to baseline by 24 hours. In a composite list of genes showing decreased expression at implantation sites and after initiation of E2-induced implantation, Reese et al. identified 21 immune-related genes, of which 14 are classical *Ig* genes (Table III in ref. 26). Strikingly, 10 of those 14 *Ig* genes are also represented in cluster 3 of our P4 time series experiments, with another 3 present in the next most closely related cluster, cluster 6. Analysis of sequence similarity amongst the probe sets representing these genes indicates that their co-regulation is unlikely to be explained by cross-hybridization alone (12).

The fact that so many of the same *Ig* genes were identified in both studies, albeit in different contexts, has interesting implications concerning the role of B cells in implantation. As proposed by Medawar (28), a key requirement for establishment of an appropriate uterine implantation environment, in which the implanting blastocyst resembles an allograft, is the induction of a state of immune tolerance. Although much attention has focused on the role of T cells and cellular immunity during implantation (reviewed in ref. 29), less is known about the regulation of B cell function. Interestingly, while the PR is expressed in B lymphocytes (30), a prior study did not identify major changes in the number of intra-uterine B cells following E2 or E2 plus P4 in either wild type or PRKO mice (31). Further experiments are required to

determine whether P4 mediates local uterine B cell function by regulating *Ig* family gene expression rather than by controlling B cell number.

Hoxa-10 is required for P4 mediated stromal cell proliferation and CKI repression

The proliferation of stromal cells and their subsequent differentiation into decidual cells are critical events in peri-implantation uterine development. In this regard, a key finding was that two cyclin dependent kinase inhibitor (CKI) genes, *p15* and *p57*, were aberrantly expressed in the *Hoxa-10* mutant uterine stroma. Interestingly, *p57* exhibits similar diffuse stromal expression in both wild type and mutant, but its expression is quantitatively more abundant in the *Hoxa-10* mutant. In contrast, *p15* undergoes a marked shift in its expression from a predominantly myometrial and submyometrial distribution in the wild type uterus to a diffuse stromal pattern in the *Hoxa-10* mutant.

The altered expression of *p15* and *p57* in the *Hoxa-10* mutant is notable. High expression levels of these CKIs during early G_0/G_1 can induce cell cycle arrest, as p15 and its family members act as specific inhibitors of the cyclin D-dependent kinases cdk4 and cdk6 (32). p57 family members show similar interactions albeit with a broader range of cyclin-cdk complexes (32). The potential functional roles of *p15* and *p57* are especially relevant as cyclin D3 associates with cdks 4 and 6, and cyclin D3 is the major $G_1 \rightarrow S$ cell cycle regulator in the peri-implantation uterine stroma (33). Interestingly, in the context of myelomonocytic cell differentiation, *Hoxa-10* directly up-regulates expression of the CKI *p21* and induces differentiation (34). In contrast, in implantation we suggest that it is the quantitative or spatially restricted repression of CKIs such as *p57* and *p15* by *Hoxa-10*, be it direct or indirect, that could explain the stromal cell proliferation defect in *Hoxa-10* mutants. *p57* null mutants die within 10

days of birth, and are thus uninformative for the consequences of *p57* loss of function in the uterus; *p15* knockout mice exhibit no uterine phenotype, and are even fertile. However, as these results pertain only to loss of function, the functional significance of the increased CKI expression observed in the *Hoxa-10* mutant uterus remains open.

The *Hoxa-10* mutant uterine stroma exhibits aberrant lymphoproliferation

A third key finding in the expression profiling experiments was that of increased transcript levels of various T cell genes. While the absolute expression of these genes on a per cell basis may be altered, the increased number of T cells in the mutant stroma as demonstrated by flow cytometry is in qualitative agreement with the increased levels of T cell related transcripts in the mutant. Moreover, flow cytometry analyses indicated an increased proliferation rate of these cells.

The lymphoproliferation observed in the *Hoxa-10* mutant uterine stroma is polyclonal and occurred after both syngeneic and allogeneic matings. These observations argue for a defect in T cell signaling, and against an antigen-specific immune response as the cause for the immune phenotype. *Hoxa-10* is expressed in early myeloid progenitors, but is not known to be present in mature neutrophils, monocytes or lymphocytes (35, 36). This is consistent with our findings that splenocytes do not express Hoxa-10 (Fig. 1B). Thus, while it remains to be formally tested whether T cells in the peri-implantation uterus express *Hoxa-10*, the available evidence suggests that the aberrant, intra-uterine lymphoproliferation in *Hoxa-10* mutants is unlikely to result from a T cell autonomous defect. Interestingly, as exemplified by Cluster 6 of the P4 time series, many chemokines, chemokine receptors and cytokines known to be mitogenic for T cells are downregulated in the uterine stroma in the presence of P4, and many of these same immunoregulatory genes are incompletely repressed by P4 in the *Hoxa-10* mutant stroma (12).

Thus, it is attractive to propose that in the mutant uterus, *Hoxa-10* deficient stromal cells stimulate the inappropriate proliferation of T cells by paracrine signaling mechanisms.

The distinct immunologic phenotype in the *Hoxa-10* mutant uterine stroma may directly cause the implantation defect in *Hoxa-10* mutant females, as the cytolytic and inflammatory activities of T cells are well known to adversely affect the viability of implanting blastocysts. Indeed, the importance of local uterine immunosuppression to normal embryo implantation and pregnancy has been observed in several mouse models. For example, in a CBA/J x DBA/2J mouse model that exhibits a high rate of spontaneous abortion mediated by a monoclonal infiltration of γδ T cells, treatment with a monoclonal antibody directed against the γδ T cell clone restores fertility (29, 37). Implantation defects are also observed in mouse models with altered uterine immunosuppression (38) and aberrant T cell proliferation (39), and these defects are abolished in lymphocyte-deficient mice, which have normal fertility. Lastly, embryonic resorption and maternal leukocyte infiltration are observed at implantation sites in the *Hoxa-10* mutant (6). Thus, the aberrant lymphoproliferation observed in the *Hoxa-10*-deficient pregnant uterus can be viewed as a localized, pro-inflammatory response that could potentially compromise pregnancy.

It is interesting to compare the abnormal immune state present in the *Hoxa-10* deficient uterus with the "pro-inflammatory" uterus described in progesterone receptor knockout (PRKO) mice (40). Experiments using the PRKO mice demonstrate that P4 acts via its receptor to antagonize the pro-inflammatory activity of estrogen, thereby decreasing the number of neutrophils and macrophages in the uterus. In contrast, the number of B lymphocytes remains unchanged (31). In the *Hoxa-10* mutant, our data suggests that P4 may act at the time of implantation through *Hoxa-10* to reduce the number of T cells in the uterus. Alternatively,

Hoxa-10 may act with the PR to co-regulate T cell number; moreover, these possibilities are not exclusive.

Although many possible mechanisms may underlie the preponderance of upregulated DRGs observed in the *Hoxa-10* mutant uterus, repressive functions have been described for both PR (41-43) and Hox proteins (44-46). Thus it is possible that Hoxa-10 may act as co-repressor and be required for transcriptional regulation by PR. Repressive functions of *Hox* genes have been described in *Drosophila* development (44) and co-repressor activity has been described for several mammalian *Hox* genes (45, 46), but mammalian targets of *Hox* gene repression, direct or indirect, have been difficult to ascertain *in vivo*. Based on their differential regulation in the *Hoxa-10* mutant uterus, we have identified several candidate *Hoxa-10* downstream genes, at least one of which, *Hoxa-11*, is also required for implantation (47). In addition, the analysis of specific DRGs in the day 3.5 p.c. pregnant uterus suggests a potential mechanism for how *Hoxa-10* regulates stromal cell proliferation. Lastly, our analyses at day 3.5 also reveal that *Hoxa-10* is required for the proper regulation of intra-uterine T cell dynamics. Both of these latter events are critical to implantation.

Materials and Methods

Mice

Disruption of the *Hoxa-10* gene was performed by insertion of a neomycin resistance cassette into an *Xho*I site within the homeobox by homologous recombination in 129/SvJ ES cells and generation of chimeric mice (5). No differences in female infertility were observed among 129/SvJ, mixed BALB/c x 129/SvJ and mixed C57BL/6 x 129/SvJ backgrounds (6). For natural matings, virginal females between 10-16 wks of age were mated with *Hoxa-10* $^{+/-}$ 129/SvJ stud males unless otherwise specified. The day of the vaginal plug was considered day 0.5 p.c. and mice were sacrificed between 7 and 9 am on days 2 – 3 p.c.

Experimental Animals

All animal experimentation described was conducted in accord with accepted standards of humane animal care. Protocols for animal work were approved by the Harvard University Institutional committee on animal care.

Western Blot Analysis

Uteri and spleens were pooled from groups of at least 3 wild type or mutant ovariectomized mice at 0, 1, 3, and 6 hours after P4 injection and placed in cold RIPA buffer containing protease inhibitor cocktail (50 μL of 25× PIC per ml RIPA buffer, Roche) on ice. Tissues were then homogenized by polytron, centrifuged at 14×g, 4°C, for 10 min; supernatant protein was quantitated by Bradford assay (Biorad), then stored at –80°C. Unless otherwise noted, 25 μg protein samples were analyzed by 10% SDS-PAGE. Following nitrocellulose transfer and blocking overnight at 4°C in 5% non-fat milk, membranes were incubated in affinity-purified

rabbit polyclonal anti-Hoxa-10 antibody at 1:300 dilution for 1 hour at RT, washed with 1× TBST (3 × 10 min), incubated with goat anti-rabbit (HRP) secondary antibody (Pharmacia), washed with TBST and incubated in ECL for 1 min. (Biorad) followed by film development. Hoxa-10 polyclonal antibody was raised in rabbits against the MAP peptide H-EEAHASSSAAEELSPAPSE-8-MAP (Research Genetics), which corresponded to a sequence in the mouse Hoxa-10 C-terminus, and affinity-purified using antigen-bound Affygel-10 (Biorad).

RNA Isolation and Oligonucleotide Microarray Hybridization

Groups of 4 wild type and 4 *Hoxa-10* mutant mice (SvJ background) at 10-16 weeks of age were ovariectomized. 14 days later, progesterone (Sigma) dissolved in sesame oil (Sigma) was injected subcutaneously (2 mg/mouse in 100 μl), followed by sacrifice of the animals and removal of uterine horns at 6 hours after injection. Care was taken to exclude the region of homeotic transformation at the uterine-oviductal junction (proximal ~25% of each uterine horn) (3). Fat and mesentery were trimmed. Tissues were snap frozen in liquid N_2, pooled, and homogenized by mortar in N_2. Total RNA was extracted using Trizol (GIBCO/BRL) according to the manufacturer's protocol, quantified by UV spectroscopy and stored in DEPC water (Ambion) in 1 μg/μl aliquots at –80°C. 0.5 μg of each RNA sample was analyzed on a 2% agarose gel to confirm integrity. Pre-chip validation of RNA collected via the OVX/P4/6h protocol was performed by assaying for up-regulation of *Hoxa-10*, *Hoxa-11* (7) and *Histidine decarboxylase* (48) as markers of P4 efficacy.

Reverse transcription used oligo-dT followed by *in vitro* transcription and biotin-labeling of cRNA (Enzo Biochem). All cRNA samples were analyzed with a Bioanalyser 2100 (Agilent Technologies) prior to chip hybridization. 20 μg of fragmented, labeled cRNA was hybridized to

Affymetrix U74A version 2 mouse oligonucleotide arrays, which were washed and scanned per Affymetrix protocol. Control samples were prepared and analyzed similarly except that sesame oil vehicle (OVX/oil/6h) rather than progesterone was injected. Triplicate pairs of wild type and mutant samples were prepared and *in vitro* transcription was performed in parallel for each of OVX/P4/6h and OVX/oil/6h RNA collections.

Data Analysis for OVX/P4/6h Wild Type vs. Mutant Comparison

Intensity and cell data were obtained using MAS 4.0.1 (Affymetrix). Data was normalized and analyzed using dChip (11) to obtain "model-based expression levels" for each probe set, upon which all subsequent analyses were performed. Criteria for significant differential expression levels between wild type and mutant were: a fold change in expression of at least 1.5, p-value of at least 0.1 (based on a t-test or other tests), and an absolute difference in expression of at least 75 units. Paired and unpaired t-tests were performed using Excel (Microsoft Office 2000, Microsoft). Expression levels from dChip were also analyzed by SAM (Significance Analysis of Microarrays), an Excel Add-in developed by Tusher et al (13), that uses a variant of the t-statistic and a permutation analysis to estimate the false positive rate within a set of significantly up- or down-regulated genes. These false positive rates take multiple hypothesis testing into account. When using paired tests with a 1.5-fold cutoff threshold and a median false detection rate of 10%, the SAM algorithm yielded similar lists of genes to those using conventional t-statistics. DRGs were classified according to their described functions based on a literature search of *PubMed* (49). A DRG was placed in more than one category if multiple functions are described.

Real Time RT-PCR

Separate aliquots of total RNA from the chip experiments were stored at –80°C. In the physiologic pregnancy model, day 3.5 p.c. total uterine RNA was pooled from 1-2 wild type or mutant mice. Samples were treated with DNaseI using the DNA-free kit (Ambion) and diluted to 20 ng/μL. Reverse transcription and quantitative PCR were performed with Superscript II Reverse Transcriptase and Taq polymerase in the One Step RT-PCR kit (Gibco BRL) on the iCycler (Biorad, Hercules, CA). No RNA and negative RT controls (no reverse transcriptase, Taq polymerase only) were included in each set of RT-PCR experiments. All samples that would be compared were tested in the same RT-PCR run. Primer and FRET (fluorescence resonance energy transfer) probe sequences were designed using Primer Express 1.0 (Applied Biosystems), purchased, or extracted from published literature. All primers were from Invitrogen and all FRET probes with 5' FAM and 3' black hole quencher labels were from Biosource. Sequences of primer and probe sets are listed in the Web Supplement (12). Threshold cycle numbers were obtained using iCycler software v2.3 (Biorad). Conditions for amplification were: RT cycle at 50°C for 15 min, 1 cycle of 95°C for 2 min, 35 cycles of 95°C for 15 sec, 59°C for 15 sec and 72°C for 15 sec. Quantitative RT-PCR reactions were performed in triplicate with total uterine RNA (Clontech) as a positive control. RNA expression levels were quantitated by comparing threshold cycles of the samples against the standard curve generated by positive controls. The experiment was valid if the negative RT controls had fluorescence intensity signals that were 100-fold less than experimental samples and if the size of the PCR products was verified by gel electrophoresis. RNA expression levels from the

ovariectomized/injection model were normalized to *Rpl-7* as a control (40), and samples from day 2.5 and 3.5 p.c. were normalized to *18S*.

RNA Sample Preparation for P4 Time Series

The mice used for the wild type P4 time series were of 129/SvImJ background (Jackson Laboratory). In the wild type P4 time series, total uterine RNA was extracted from ovariectomized mice at 0 (no injection), 1, 3, 6, 9, 12, 15, 18 and 24 hours after P4 injection. Samples containing pooled total uterine RNA from at least 4 mice were used for each time point. The time course dataset was generated in two sets, (0, 1, 3, 6, 9h) and (0, 6, 12, 15, 18, 24h). Samples in the same batch were processed in parallel at all steps, including ovariectomy, P4 injection, RNA collection, IVT labeling and chip hybridization. 0h and 6h timepoints were acquired in both batches to allow comparison between batches. The correlation between duplicates (at 0h and 6h) was much higher ($r^2 > 0.975$) than that amongst samples within the same batch. Therefore, all timepoints were merged into one dataset for analysis.

SOM Analysis Of Gene Expression In P4 Response Time Series.

dChip expression levels from experiments using wild type ovariectomized mice at 9 timepoints (0, 1, 3, 6, 9, 12, 15, 18 and 24 hours) after P4 injection were used, and only genes with at least a 2-fold change and absolute signal change of at least 75 units between any 2 time points were included in the SOM analysis (Genecluster, Whitehead Genome Center, MIT) (15). Expression profiles for 1675 genes fulfilling these criteria were normalized prior to clustering so that each gene's expression profile has mean 0 and variance 1 on the log scale. The number of nodes was incrementally increased until no further expression patterns emerged. A 3×6 geometry of nodes

is depicted in the Web Supplement. Clustering by SOM was also performed by using a 1.5-fold cutoff filter, with similar qualitative results.

Statistical Methods For Determining Functional Category Enrichment

A hypergeometric distribution was used to calculate the probability of observing the number of DRGs within each cluster in the time series. The probability *P* of observing at least *k* DRGs within a cluster of size (*n*) is:

$$P = 1 - \sum_{i=0}^{k-1} \frac{\binom{f}{i}\binom{g-f}{n-i}}{\binom{g}{n}}$$

where (*f = 119*) is the total number of probe sets representing DRGs and (*g = 12386*) is the number of probe sets representing interrogated genes on the Affymetrix U74Av2 array. Alternatively, we also calculated p-values based only on the subset of genes which passed the filtering for inclusion into the SOM clustering algorithm so that *f = 67* and *g = 1675*. A Bonferonni correction for multiple tests (m = 18, the number of clusters) was used to obtain an adjusted p-value cutoff (α') for a chosen target significance level ($\alpha = 0.05$) according to the following equation (Cheung KJ, Badarinarayana V, Selinger D, Janse D, and Church GM, Microarray analysis reveals supercoiling-dependent transcription in the *Escherichia coli* osmotic stress regulon, submitted manuscript): $\alpha' = 1 - (1 - \alpha)^{1/(m-1)}$. Setting $\alpha = 0.05$ and m = 18, α' is 0.0030.

In Situ Hybridization and Immunohistochemistry

Uteri were cut into 4-6 mm pieces and flash frozen in Histo-Freeze (Fisher Scientific, Pittsburgh, PA). Frozen sections (11 μm) were mounted onto poly-L-lysine coated slides and fixed in cold 4% paraformaldehyde in PBS. Sections were pre-hybridized and hybridized at 45°C for 4 h in

50% formamide hybridization buffer containing the ^{35}S-labeled antisense cRNA probe (specific activities ~ 2 x 10^9 dpm/μg). After hybridization and washing, sections were incubated with RNaseA (20 μg/ml) at 37°C for 20 min. RNase A-resistant hybrids were detected by autoradiography using Kodak NTB-2 liquid emulsion (Eastman Kodak Co., Rochester, NY). Sections hybridized with the corresponding sense probe served as negative controls. Slides were post-stained with hematoxylin and eosin. ^{35}S-labeled riboprobes were generated using specific RNA polymerases. An IMAGE clone of *p15* in pCMV-SPORT6 (IMAGE clone 3495097, Genbank Accession #BC002010) was purchased from Research Genetics and confirmed by sequencing. Plasmid for the *p57* riboprobe was a generous gift from Dr. Stephen Elledge.

For immunohistochemistry, uteri were cut into 4-6 mm pieces and flash frozen in Histo-Freeze (Fisher Scientific, Pittsburgh, PA). Frozen sections (12 μm) were mounted onto poly-L-lysine coated slides and fixed in Bouin's fixative and washed in PBS. Immunostaining with the primary antibody (anti-CD4, H129.9, Pharmingen) was performed using Zymed Histostain kit following manufacturer's protocol.

Flow Cytometric Analysis of Uterine Stromal Cells and Splenocytes

Uterine stromal cells (USC) were isolated from groups of 4-5 wild type and *Hoxa-10* mutant mice on day 2.5 or 3.5 p.c. as specified. In each group, uteri excluding the utero-oviductal junction were excised, trimmed of fat and mesentery, rinsed in PBS, flushed of embryos, pooled and minced into fine fragments. 4 rounds of 5-min. incubation using collagenase type I (Sigma), mechanical disruption by pipetting, 5-min. sedimentation by gravity followed by removal of supernatant were performed in serum-free DMEM/F-12 (Gibco) containing 1% penicillin-streptomycin (Sigma). Supernatant containing isolated USC was passed through a 70 μm cell

strainer (Falcon, BD) to remove cell clumps. Cell suspensions were centrifuged at 1400 rpm, 4°C, for 5 min. and USC re-suspended in FACS buffer (PBS, 0.5% Bovine Serum Albumin, 0.02% sodium azide) on ice.

Spleens were removed and pooled from the same groups of mice and kept in PBS with 5% FCS on ice. Splenocytes were prepared by homogenization of the spleen capsule using the plunger end of a syringe, passed through a 70 μm cell strainer and suspended in PBS containing 5% FCS. Cells were pelleted by centrifugation (1800 rpm, 4°C, 5 min.), re-suspended in ACK buffer (0.15M NH_4Cl, 1.0mM $KHCO_3$ and 0.1mM Na_2EDTA) for 5 minutes to lyse RBCs, re-pelleted by centrifugation and re-suspended in FACS buffer. 100 μL of USC or splenocyte suspension was incubated with normal rabbit serum (Pharmingen) at 1:50 dilution for 5 min. on ice, followed by centrifugation and aspiration of supernatant. Cell pellets were resuspended in 50 μL of directly fluorochrome-conjugated monoclonal antibodies diluted in FACS buffer to a concentration of 0.1 mg/ml for 30 min. in the dark on ice. Cells were washed twice in FACS buffer and analyzed on a FACScan (Becton Dickinson) with Cellquest software within 2 hours of staining. The monoclonal antibodies used were (BD, Pharmingen): FITC-anti-gamma delta TCR (GL3), FITC-anti-TCR beta (H57-597), FITC-anti-Pan-NK (DX5), FITC-anti-CD19 (1D3), FITC-anti-CD4 (H129.9), PE-anti-gamma delta TCR (GL3), PE-anti-TCR beta (H57-597), PE-anti-Pan-NK (DX5), PE-anti-CD19 (1D3) and PE-anti-CD4 (H129.9).

Cell Proliferation

4 hours prior to the sacrifice of mice, 100 μL (1 mg) of bromodeoxyuridine (BrdU, BD Biosciences) was injected i.p. into each mouse. Cell staining was performed as above followed by cell fixing, permeabilization, DNase treatment and BrdU staining using the BrdU Flow Kit

(BD Biosciences) according to the manufacturer's protocol. Fixed and stained cells were kept in FACS buffer in 4°C overnight and analyzed by FACS the next morning.

Acknowledgments

We thank S. Stowell, S. Heaney; J. Shan, and W. Lu; J. Couget (Harvard Center for Genomics Research) for assistance with Affymetrix chip hybridizations; S.K. Dey, J. Comander and S. Mok for valuable discussions; C. Mak, L. Wu, M. Ramoni and I. Kohane for advice on statistics, and D. Gould and J. LaVecchio for help with flow cytometry. This work was supported by NIH grants RO1HD35580 and PO1GM61354 (RM), RO1HD40810 (HL), K12HD01255 (DS), DOE grant DE-FG02-87-ER60565 (GC) and an ACOG-Ortho McNeil Research Fellowship (MY).

References

1. See http://www.asrm.org and material therein.
2. Paria BC, Reese J, Das, SK, Dey SK 2002 Molecular signaling in uterine receptivity for implantation. Science 296:2185-2188
3. Ma L, Yao M, Maas RL 1999 Genetic control of uterine receptivity during implantation. Semin Reprod Endocrinol 17:205-216
4. Benson GV, Nguyen ET-H, Maas RL 1995 The expression pattern of the murine *hoxa-10* gene and its sequence recognition of its homeodomain reveal specific properties of *Abdominal B*-like genes. Mol Cell Biol 15:1591-1601
5. Satokata I, Benson G, Maas R 1995 Sexually dimorphic sterility phenotypes in *Hoxa-10*-deficient mice. Nature 374:460-463
6. Benson GV, Lim H, Paria BC, Satokata I, Dey SK, Maas RL 1996 Mechanisms of reduced fertility in *Hoxa-10* mutant mice: uterine homeosis and loss of maternal *Hoxa-10* expression. Development 122:2687-2696
7. Ma L, Benson GV, Lim H, Dey SK, Maas RL 1998 *Abdominal B (AbdB) Hoxa* genes: regulation in adult uterus by estrogen and progesterone and repression in Müllerian duct by the synthetic estrogen diethylstilbestrol (DES). Dev Biol 197:141-154
8. Lim H, Ma L, Ma WG, Maas RL, Dey SK 1999 *Hoxa-10* regulates uterine stromal cell responsiveness to progesterone during implantation and decidualization in the mouse. Mol Endocrinol 13:1005-1017
9. Duboule D 1995 Vertebrate *Hox* genes and proliferation: an alternative pathway to homeosis? Curr Opin Genet Dev 5:525-528.

10. Capecchi MR 1997 Hox genes and mammalian development. CSH Symp Quant Biol LXII: 273-281
11. Li C, Wong WH 2001 Model-based analysis of oligonucleotide arrays: expression index computation and outlier detection. Proc Natl Acad Sci USA 98:31-36
12. Web supplemental data accessible at: http://genetics.med.harvard.edu/~schoe/mylene/web.supplement/index.htm
13. Tusher VG, Tibshirani R, Chu G 2001 Significance analysis of microarrays applied to the ionizing radiation response. Proc Natl Acad Sci USA 98:5116-5121
14. Furlong EEM, Andersen EC, Null B, White KP, Scott MP 2001 Patterns of gene expression during *Drosophila* mesoderm development. Science 293:1629-33
15. Edgar R, Domrachev M, Lash AE 2002 Gene expression omnibus: NCBI gene expression and hybridization array data repository. Nucleic Acids Research 30:207-210
16. Data series GSE108 (OVX/P4/6h/UTX 129 WT vs. Hoxa-10-/-) can be accessed at Gene Expression Omnibus http://www.ncbi.nlm.nih.gov/geo
17. Data series GSE109 (OVX/oil/6h/UTX 129 WT vs. Hoxa-10-/-) can be accessed at Gene Expression Omnibus http://www.ncbi.nlm.nih.gov/geo
18. Data series GSE106 (OVX/P4/UTX 129/SvImJ WT A) and GSE107 (OVX/P4/UTX 129/SvImJ WT B) can be accessed at Gene Expression Omnibus http://www.ncbi.nlm.nih.gov/geo
19. Tamayo P, Slonim D, Mesirov J, Zhu Q, Kitareewan S, Dmitrovsky E, Lander ES, Golub TR 1999 Interpreting patterns of gene expression with self-organizing maps: methods and application to hematopoietic differentiation. Proc Natl Acad Sci USA 96:2907-2912

20. Tavazoie S, Hughes JD, Campbell MJ, Cho RJ, Church GM 1999 Systematic determination of genetic network architecture Nat Genet 22:281-285

21. Gellon G, McGinnis W 1998 Shaping animal body plans in development and evolution by modulation of Hox expression patterns Bioessays 20:116-25

22. Maconochie MK, Nonchev S, Studer M, Chan SK, Popperl H, Sham MH, Mann RS, Krumlauf R 1997 Cross-regulation in the mouse HoxB complex: the expression of Hoxb2 in rhombomere 4 is regulated by Hoxb1 Genes Dev 11:1885-95

23. Taylor HS, Igarashi P, Olive DL, Arici A 1999 Sex steroids mediate *Hoxa11* expression in the human peri-implantation endometrium. J Clin Endocrinol Metab 84:1129-1135

24. Yoshioka K-I, Matsuda F, Takakura K, Noda Y, Imakawa K, Sakai S 2000 Determination of genes involved in the process of implantation: application of GeneChip to scan 6500 genes. Biochem Biophys Res Comm 272:531-538

25. Kao LC, Tulac S, Lobo S, Imani B, Yang JP, Germeyer A, Osteen K, Taylor RN, Lessey BA, Giudice LC 2002 Global gene profiling in human endometrium during the window of implantation. Endocrinology 143:2119-2138.

26. Reese J, Das SK, Paria BC, Lim H, Song H, Matsumoto H, Knudtson KL, DuBois RN, Dey SK 2001 Global gene expression analysis to identify molecular markers of uterine receptivity and embryo implantation. J Biol Chem 276:44137-44145

27. Gething MJ 1999 Role and regulation of the ER chaperone BiP. Semin Cell Dev Biol 10:465-472

28. Medawar PB 1953 Some immunological and endocrinological problems raised by evolution of viviparity in vertebrates. Symp Soc Exp Biol 7:320-328

29. Arck PC, Ferrick DA, Steele-Norwood D, Egan PJ, Croitoru K, Carding SR, Dietl J, Clark DA 1999 Murine T cell determination of pregnancy outcome. Cell Immunol 196:71-79
30. Pasanen S, Ylikomi T, Palojoki E, Syvala H, Pelto-Huikko M, Tuohimaa P 1998 Progesterone receptor in the chicken of Fabricius and thymus: evidence for expression in B-lymphocytes. Mol Cell Endocrinol 141:19-128
31. Tibbetts TA, Conneely OM, O'Malley BW 1999 Progesterone via its receptor antagonizes the pro-inflammatory activity of estrogen in the mouse uterus. Biol Reprod 60:1158-1165
32. Malumbres M, Ortega S, Barbacid M 2000 Genetic analysis of mammalian cyclin-dependent kinases and their inhibitors. Biol Chem 381:827-838
33. Tan J, Raja S, Davis MK, Tawfik O, Dey SK, Das SK 2002 Evidence for coordinated interaction of cyclin D3 with p21 and cdk6 in directing the development of uterine stromal cell decidualization and polyploidy during implantation. Mech Dev 111:99-113
34. Bromleigh VC, Freedman LP 2000 p21 is a transcriptional target of HOXA10 in differentiating myelomonocytic cells. Genes Dev 14:2581-2586
35. Lawrence HJ, Sauvageau G, Ahmadi N, Lopez AR, LeBeau MM, Link M, Humphries K, Largman C 1995 Stage- and lineage-specific expression of the HOXA10 homeobox gene in normal and leukemic hematopoietic cells. Exp Hematol 23:1160-1166
36. Thorsteinsdottir U, Sauvageau G, Hough MR, Dragowska W, Lansdorp PM, Lawrence HJ, Largman C, Humphries RK 1997 Overexpression of HOXA10 in murine hematopoietic cells perturbs both myeloid and lymphoid differentiation and leads to acute myeloid leukemia. Mol Cell Biol 17:495-505

37. Gorivodsky M, Zemlyak I,Orenstein H, Savion S, Fein A, Torchinsky V, Toder J 1998 TNF-alpha messenger RNA and protein expression in the uteroplacental unit of mice with pregnancy loss. J Immunol 160:4280-4288

38. Makrigiannakis A, Zoumakis E, Kalantaridou S, Coutifaris C, Margioris AN, Coukos G, Rice KC, Gravanis A, Chrousos GP 2001 Corticotropin-releasing hormone promotes blastocyst implantation and early maternal tolerance. Nat Immunol 2:1018-1024

39. Munn DH, Zhou M, Attwood JT, Bondarev I, Conway SJ, Marshall B, Brown C, Mellor AL 1998 Prevention of allogeneic fetal rejection by tryptophan catabolism. Science 281:1191-1193

40. Lydon JP, DeMayo FJ, Funk CR, Mani SK, Hughes AR, Montgomery CA, Shyamala G, Conneely OM, O'Malley BW 1995 Mice lacking progesterone receptor exhibit pleiotropic reproductive abnormalities. Genes Dev 9:2266-2278

41. Xu J, Nawaz Z, Tsai SY, Tsai M-J, O'Malley BW 1996 The extreme C terminus of progesterone receptor contains a transcriptional repressor domain that functions through a putative corepressor. Proc Natl Acad Sci USA 93:12195-12199

42. Giangrande PH, Kimbrel EA, Edwards DP, McDonnell DP 2000 The opposing transcriptional activities of the two isoforms of the human progesterone receptor are due to differential cofactor binding. Mol Cell Biol 20:3102-3115

43. Mulac-Jericevic B, Mullinax RA, DeMayo FJ, Lydon JP, Conneely OM 2000 Subgroup of reproductive functions of progesterone mediated by progesterone receptor-B isoform. Science 289:1751-1754

44. Appel B, Sakonju S 1993 Cell-type-specific mechanisms of transcriptional repression by the homeotic gene products UBX and ABD-A in *Drosophila* embryos. EMBO J 12:1099-1109

45. Saleh M, Rambaldi I, Yang X-J, Featherstone MS 2000 Cell signaling switches HOX-PBX complexes from repressors to activators of transcription mediated by histone deacetylases and histone acetyltransferases. Mol Cell Biol 20:8623-8633

46. Shi X, Bai S, Li L, Cao X 2001 Hoxa-9 represses transforming growth factor-ß-induced osteopontin gene transcription. J Biol Chem 276:850-855

47. Gendron RL, Paradis H, Hsieh-Li HM, Lee DW, Potter SS, Markoff E 1997 Abnormal uterine stromal and glandular function associated with maternal reproductive defects in Hoxa-11 null mice. Biol Reprod 56:1097-1105

48. Paria BC, Das N, Das SK, Zhao X, Dileepan KN, Dey SK 1998 Histidine decarboxylase gene in the mouse uterus is regulated by progesterone and correlates with uterine differentiation for blastocyst implantation. Endocrinol 139:3958-3966

49. http://www.ncbi.nlm.nih.gov/PubMed/

Table 1A. Summary of DRG identification by SAM and t test.

	No. Genes Identified by:			
	SAM	t test	Both SAM and t test	**SAM and/or t test**
Higher Expression in Wild Type	15	23	12	**26**
Higher Expression in Mutant	77	58	45	**90**
Total No. DRGs*	**92**	**81**	**57**	**116**

* The total number of 116 DRGs was represented by 119 probesets because in 3 cases, 2 probesets represented the same DRG.

Table 1B. Genes that have significantly higher uterine expression levels in the wild type compared to *Hoxa-10* mutant at 6 hours after P4 injection in ovariectomized mice (15, 16).

Probe Set ID	Gene Name	Statistical Tests	
		Fold Change by SAM	Paired t test
98817_at	follistatin	* 4.91	*
92970_at	homeo box A10	* 3.49	*
99926_at	polymeric immunoglobulin receptor	* 2.68	
98577_f_at	endogenous retroviral sequence 4 (with leucine t-RNA primer)	* 2.54	*
93860_i_at	Mouse endogenous murine leukemia virus modified polytropic provirus†	* 2.48	*
93861_f_at	Mouse endogenous murine leukemia virus modified polytropic provirus†	* 2.22	*
100381_at	actin, alpha 1, skeletal muscle	* 2.11	*
92796_at	alkaline phosphatase 2, liver	* 2.04	*
92852_at	fibronectin 1	1.82	*
99637_at	procollagen, type XV	1.81	*
101900_at	cyclin-dependent kinase inhibitor 2B (p15, inhibits CDK4)	* 1.75	*
161670_f_at	EST Mus musculus cDNA, GB No. AV140884	* 1.73	*
100064_f_at	gap junction membrane channel protein alpha 1	* 1.72	*
96602_g_at	EST Mus musculus cDNA, 3 end /clone=UI-M-BH1-akt-a-08-0-UI	1.70	*
161595_at	EST Mus musculus cDNA, GB No. AV292586	* 1.66	*
104480_at	cathepsin L	1.65	*
93873_s_at	homeo box A11, opposite strand transcript	* 1.63	*
102259_at	3-monooxgenase/tryptophan 5-monooxgenase activation protein, gamma	* 1.63	
103049_at	M.musculus N-myc gene, 3 end; MoMuLV-like endogenous provirus	1.63	*
101294_g_at	glucose-6-phosphate dehydrogenase 2	1.62	*
104021_at	homeo box A11	* 1.61	*
160899_at	Purkinje cell protein 4	1.59	*
101707_at	alcohol dehydrogenase family 1, subfamily A7	1.56	*
160376_at	EST Mus musculus cDNA, clone=UI-M-BH2.2-aqm-e-10-0-UI	1.56	*
95246_at	EST Mus musculus cDNA, GB No. AA516958	* 1.51	
102637_at	transforming growth factor, beta receptor III	1.48	*
160923_at	EST Mus musculus cDNA, clone=IMAGE-1478803	1.45	*

These genes have significantly different uterine expression levels in *Hoxa-10* wild type compared to mutant in the OVX/6h/P4 model by paired analysis in SAM, conventional t test, or both. "*" indicates statistical significance based on the following criteria. t test: fold change of at least 1.5, p-value of at least 0.1, an absolute difference in expression of at least 75 units. SAM: fold change of at least 1.5 in paired testing and median false detection rate of 10%.

† Two probesets representing the same gene were identified.

Table 1C. Genes that have significantly higher uterine expression levels in the *Hoxa-10* mutant compared to wild type at 6 hours after P4 injection in ovariectomized mice (15, 16).

Probe Set ID	Gene Name	Statistical Test	
		Fold Change by SAM	Paired t test
160375_at	EST Mus musculus cDNA, GB No. AJ006474	* 3.09	*
103238_at	wingless-related MMTV integration site 4	* 3.00	*
94057_g_at	Cluster Incl M21285:Stearoyl-coenzyme A desaturase 1 †	* 2.67	*
99671_at	adipsin	* 2.61	*
101115_at	lactotransferrin	* 2.46	*
99104_at	adipocyte complement related protein of 30 kDa	* 2.42	*
102798_at	adrenomedullin	* 2.41	*
94056_at	Cluster Incl M21285:Stearoyl-coenzyme A desaturase 1 †	* 2.38	*
160852_at	keratin complex 1, acidic, gene 15	* 2.37	*
97402_at	thioether S-methyltransferase	* 2.08	*
102823_at	immunoglobulin heavy chain 3 (serum IgG2b) †	* 2.08	
93996_at	cytochrome P450, 2e1, ethanol inducible	* 2.07	*
161354_f_at	EST Mus musculus cDNA, GB No. AV161034	* 2.00	*
99369_f_at	immunoglobulin kappa light chain variable region precursor (Vk10c) gene	* 1.97	
103538_at	DNA segment, Chr 5, ERATO Doi 189, expressed	* 1.92	*
92805_s_at	ADP-ribosylation-like 4	* 1.86	
102824_g_at	immunoglobulin heavy chain 3 (serum IgG2b) †	* 1.86	
160173_at	EST Mus musculus cDNA, GB No. AI852838	* 1.86	
93855_at	rad and gem related GTP-binding protein	* 1.82	*
100334_f_at	kallikrein 13	* 1.81	*
93515_at	cadherin 16	* 1.78	
96088_at	N-myc downstream regulated 2	* 1.78	*
101947_at	neighbor of A-kinase anchoring protein 95	* 1.72	*
102725_at	potassium voltage gated channel, shaker related subfamily, beta member 1	* 1.72	
104469_at	glycoprotein 38	* 1.72	*
93198_at	colony stimulating factor 3 receptor (granulocyte)	* 1.67	
98792_at	EST Mus musculus cDNA, GB No. W51672	* 1.67	*
93486_at	solute carrier family 27 (fatty acid transporter), member 1	* 1.66	
104242_f_at	EST Mus musculus cDNA, GB No. AI835622	* 1.65	
96765_at	paternally expressed gene 3	* 1.65	
98453_at	FMS-like tyrosine kinase 1	* 1.64	
101578_f_at	actin, beta, cytoplasmic	* 1.64	
95356_at	apolipoprotein E	* 1.63	*
103819_at	src homology 2 domain-containing transforming protein D	* 1.63	
97950_at	xanthine dehydrogenase	* 1.62	*
100050_at	inhibitor of DNA binding 1	* 1.61	*
100998_at	histocompatibility 2, class II antigen A, beta 1	* 1.61	*
95471_at	cyclin-dependent kinase inhibitor 1C (P57)	* 1.60	*
95759_at	stearoyl-Coenzyme A desaturase 2	* 1.60	*
93615_at	pre B-cell leukemia transcription factor 3	* 1.60	

96825_at	EST Mus musculus cDNA, GB No. AI854794	*	1.60	*
99481_at	ATPase, Na+/K+ transporting, alpha 2 polypeptide	*	1.60	
101969_at	neuroblastoma, suppression of tumorigenicity 1	*	1.60	*
98960_s_at	UDP-Gal:betaGlcNAc beta 1,3-galactosyltransferase, polypeptide 3	*	1.59	*
100069_at	cytochrome P450, 2f2	*	1.59	*
99187_f_at	EST Mus musculus cDNA, GB No. AI835662	*	1.59	*
103954_at	rat generating islet-derived, mouse homolog 3 alpha	*	1.59	*
160373_i_at	EST Mus musculus cDNA, GB No. AI839175	*	1.59	*
95082_at	insulin-like growth factor binding protein 3	*	1.58	*
96907_at	DNA segment, Chr 8, Wayne State University 96, expressed	*	1.58	
161610_at	N-myc downstream regulated 2	*	1.57	*
102157_f_at	Ig V-kappa10-Ars-A kappa chain gene, complete cds	*	1.57	
102371_at	nuclear receptor subfamily 4, group A, member 1	*	1.57	*
92836_at	EST Mus musculus cDNA, 5 end /clone=IMAGE-1316437		1.56	*
93015_at	glutathione S-transferase, alpha 3	*	1.56	
99828_at	EST Mus musculus cDNA, GB No. AA673252	*	1.56	
95019_at	glutathione S-transferase, theta 1	*	1.56	*
101082_at	malic enzyme, supernatant	*	1.55	
100153_at	neural cell adhesion molecule	*	1.55	
160905_s_at	hypothetical protein MNCb-2875	*	1.55	
97548_at	FK506-binding protein 3 (25kD)	*	1.55	
96592_at	phosphatidylinositol 3-kinase, p85 alpha regulatory subunit	*	1.53	*
98790_s_at	myeloid ecotropic viral integration site 1	*	1.53	*
100431_at	leptin receptor	*	1.53	*
161310_at	EST Mus musculus cDNA, GB No. AV079187	*	1.53	
92245_at	EST Mus musculus cDNA, GB No. AI642262	*	1.52	
96038_at	ribonuclease, RNase A family 4	*	1.52	*
97835_at	EST AI303516	*	1.52	*
101593_at	nudix (nucleotide diphosphate linked moiety X)-type motif 3	*	1.52	*
98868_at	Cluster Incl L31532:B-cell leukemia/lymphoma 2	*	1.51	
99067_at	growth arrest specific 6	*	1.51	*
102744_at	T-cell receptor gamma, variable 4	*	1.51	
160306_at	thyroid hormone responsive SPOT14 homolog (Rattus)	*	1.51	
160841_at	D site albumin promoter binding protein	*	1.51	
97317_at	ectonucleotide pyrophosphatase/phosphodiesterase 2	*	1.50	*
104000_at	EST Mus musculus cDNA, GB No. AI181346	*	1.50	*
104285_at	3-hydroxy-3-methylglutaryl-Coenzyme A reductase	*	1.50	
104601_at	thrombomodulin	*	1.50	
92366_at	laminin, alpha 2	*	1.50	
160564_at	lipocalin 2	*	1.49	*
92534_at	GTP binding protein (gene overexpressed in skeletal muscle)	*	1.48	*
99603_g_at	TGFB inducible early growth response		1.48	*
104516_at	claudin 5		1.48	*
104716_at	retinol binding protein 1, cellular		1.48	*
160834_at	EST Mus musculus cDNA, clone=UI-M-AP1-agn-a-04-0-UI		1.48	*

161907_s_at	tenascin X	1.47	*
93527_at	Kruppel-like factor 9	1.47	*
104217_at	EST Mus musculus cDNA, clone=UI-M-BH1-akt-a-10-0-UI	1.47	*
93330_at	aquaporin 1	1.46	*
95693_at	isocitrate dehydrogenase 2 (NADP+), mitochondrial	1.46	*
96148_at	EST Mus musculus cDNA, clone=UI-M-AL1-ahk-f-10-0-UI	1.46	*
104728_at	protein S (alpha)	1.44	*

Table 2. Functional categories of DRGs.

No. of DRGs	Functional Category
16	Immune Function / Complement system / Cytokine-related
16	Enzyme / Metabolism
13	Adipocyte function / Fat metabolism / Energy balance
9	Transcription regulation / transcription factors
8	Cell cycle / Cell proliferation
7	TGF beta signaling pathway
6	Ras-related small GTP-binding proteins / GTPase Superfamily
2	Cell-cell junction
4	Cell adhesion / Integrin
6	Signaling protein / mesenchymal-epithelial signaling
3	Cytoskeletal / Structural
3	Ion or water channels / regulation of intracellular osmotic content
1	Golgi function / regulation of intracellular transport / vesicular transport
1	Nuclear / DNA-binding proteins
1	Iron utilization
1	Protease
2	Murine Virus
1	Novel Gene
1	Apoptosis Inhibitor
1	Blood Clotting Factor
44	Unknown genes / ESTs

DRGs were classified according to their described functions based on literature search on PubMed (49). A DRG was placed in more than one category if multiple functions have been described. See Web Supplement for complete list of DRGs in each functional category (12).

Table 3. DRG enrichment of SOM clusters identifies co-regulation of genes by Hoxa-10 and P4 (15, 18).

Cluster	No. DRG Probesets	No. Probesets in Cluster	P-value
0	7	92	7.03E-02
1	12	88	1.16E-04 *
2	4	108	6.39E-01
3	1	51	8.79E-01
4	0	23	1.00E+00
5	7	36	3.96E-04 *
6	15	98	3.09E-06 *
7	4	82	4.18E-01
8	5	58	7.85E-02
9	2	91	8.90E-01
10	0	77	1.00E+00
11	2	115	9.53E-01
12	4	83	4.27E-01
13	0	190	1.00E+00
14	1	162	9.99E-01
15	1	36	7.74E-01
16	1	89	9.76E-01
17	1	196	1.00E-01

1675 probesets had a minimum relative fold difference > 2 and a minimum absolute difference of 75 units in expression levels between 2 time points and were cluster analyzed by SOM using Genecluster (20). For each cluster, p-values based on a hypergeometric distribution were calculated using the the number of probesets representing DRGs (DRG probesets) and the total number of probesets in that cluster (Probesets in Cluster). The significant enrichment for DRGs in Clusters 1, 5 and 6 (denoted by *) supports the co-regulation of these DRGs by Hoxa-10 and P4 ($p<0.0030$).

Figure Legends

Figure 1. Experimental strategy. **(A)** Protocol for gene expression profiling and experimental evaluation of differentially regulated genes (DRGs) in the *Hoxa-10* mutant uterus. **(B)** Total uterine protein extracts collected at 0, 1, 3 and 6 hrs. after P4 injection in ovariectomized wild type mice show significant up-regulation of Hoxa-10 protein (~55Kd) by 6 hours. Subsequent levels were constant, declining by 24 h (not shown). Lane 1, positive control (10 μg of protein extract from U2OS cells transfected with *Hoxa-10* expression plasmid driven by CMV promoter); lane 2, no sample loaded; lanes 3-9 were each loaded with 25 μg of protein extract except for lane 5 (40 μg). Abbr. WT: wild type; MUT: *Hoxa-10* mutant; S: spleen.

Figure 2. Co-regulation of *Hoxa-11* expression by Hoxa-10 and P4. **(A)** *Hoxa-11* expression in response to oil and P4 injections in wild type mice at 0, 1, 3, 6 and 9 hrs. The differences in *Hoxa-11* expression in P4-injected compared to oil-injected mice are 2.3, 2.2, 10.5 and 3.6-fold, respectively ($p < 0.05$ for each time point). **(B)** Attenuation of *Hoxa-11* expression levels in the *Hoxa-10* mutant mice at 6h after P4 injection. In 4 independent experiments, *Hoxa-11* was more highly expressed in the wild type than *Hoxa-10* mutant by 1.6, 1.5, 1.3 and 3.1-fold, respectively. Overall, wild type *Hoxa-11* expression was 1.9-fold higher than mutant (2.5 ± 0.2 vs. 1.5 ± 0.1; mean ± SEM) ($p=0.01$). In all bar graphs, each bar represents the mean of triplicate measurements of a sample comprised of pooled uterine RNA from 4 mice of the indicated genotype. Error bars for data points with SEM < 0.05 are not visible. All gene expression levels in Fig. 2 were normalized to *Rpl-7* expression levels. Student's 2-tailed t test was used to test for statistical significance, and paired t test was used when appropriate.

Figure 3. Representative clusters from SOM analysis of P4 time series. **(A)** SOM Cluster 3 from the wild type time series showed significant enrichment of immunoglobulin genes. 40 of the 51 genes (78%) in this cluster were immunoglobulin genes expressed by B lymphocytes. The results demonstrate powerful clustering of co-regulated genes in the wild type P4 time series by SOM, independent of DRGs. The upper, middle and lower lines represent the 90^{th}, 50^{th} and 10^{th} percentile of the expression level at each time point. **(B)** Wild type P4 time series SOM clusters with significant enrichment of DRGs. Wild type P4 time series Clusters 1, 5 and 6 had significant enrichment with DRGs (See Table 2). Cluster 6 is especially interesting as it represents genes whose repression was immediate and then persisted for 24 hours. [See Web Supplement for all SOM clusters of the P4 time series (12)].

Figure 4. Defective regulation of CKI genes and stromal cell proliferation in the *Hoxa-10* mutant. **(A)** Expression of *p15* and *p57* in the day 3.5 p.c. *Hoxa-10* mutant uterus. Quantitative real time RT-PCR showed higher expression levels of *p57* (6.6 ± 1.8 fold) in the mutant compared to wild type on day 3.5 p.c. (*p=0.08 based on paired t test of log transformed data). In contrast, although *p15* expression was increased by 3.1 ± 1.2 fold in the mutant, the increase was not significant. Data represents the mean ± SEM of the mutant to wild type expression ratio from 3 independent experiments. All expression levels were normalized to *18S*. **(B)** *In situ* hybridization showing redistribution of *p15* expression in the *Hoxa-10* mutant uterus. On day 3.5 p.c., *p15* is expressed predominantly in the myometrium (M) and submyometrial stroma (bright stain that is parallel to the myometrial signal) in the wild type uterus, with low expression in the stroma (S) underlying the luminal epithelium (LE). In contrast, in the *Hoxa-10* mutant, expression is present throughout the entire uterine stroma (40×). Similar results were observed in

3 wild type and 3 *Hoxa-10* mutant mice, and in the OVX/P4/6h model. **(C).** Decreased uterine stromal cell proliferation in the day 3.5 p.c. *Hoxa-10* mutant. The proportion of stromal cells that have undergone cell proliferation was significantly less in the mutant (5.7 ± 0.2%; mean ± SEM) than in wild type (8.9 ± 0.1%) in 4 replicates; $p<0.01$. Data are analysed based on M1 ~ 5% $BrdU^+$ (background) in the no stain control. Coordinates of M1 are set to be the same in the no stain and BrdU histograms for each of wild type and mutant. Results shown are representative of four replicates in one experiment. The experiment was performed a total of 3 times with similar results.

Figure 5. Relative T cell number increase in the peri-implantation *Hoxa-10* mutant uterus. **(A)** The proportion of each lymphocyte subpopulation in the uterine stroma was greater in mutant compared to wild type on day 3.5 p.c. by flow cytometry. On day 2.5 p.c., the proportions of $CD4^+$ and $TCR\gamma\delta^+$ populations were 1.4 ± 0.0 (mean ± SEM) and 2.4 ± 0.1 times greater in the mutant uterus, respectively. On day 3.5 p.c., the $CD4^+$, $CD8^+$, $TCR\gamma\delta^+$, $TCR\alpha\beta^+$, and NK cells ($DX5^+$) populations were 2.5 ± 0.1, 3.2 ± 0.1, 2.3 ± 0.2, 1.9 ± 0.1 and 2.2 ± 0.1 times greater in the mutant uterus compared to wild type, respectively (*$p<0.01$ and $^{\dagger}p<0.05$ in paired t-tests comparing the mutant to wild type ratio for uterus to that of spleen control). Spleen controls showed a mutant to wild type ratio of ~1 for all cell populations. All data analyses for Fig. 5 were performed using a lymphocyte gate set by inclusion of >90% of $CD3^+$ and $CD4^+$ cells, or by using the lymphocyte gate from spleen samples within the same experiments. **(B)** Increased percentage of single and double positive $CD4^+$ with $TCR\gamma\delta^+$ or $TCR\alpha\beta^+$ cells in day 3.5 p.c. mutant stroma. *Upper panel:* Flow cytometry dotplots showing the $TCR\gamma\delta^+$ versus $CD4^+$ T cell markers in uterine stromal cells isolated from wild type and mutant on day 3.5 p.c. with

splenocytes as control. *Lower panel:* Flow cytometry dotplots showing the TCR$\alpha\beta^+$ versus $CD4^+$ T cell markers. The number in each quadrant is the percentage of cells in the lymphocyte gate. Dotplots are representative of 3 experiments for each of day 2.5 and 3.5 p.c. tissues. **(C)** Immunostaining showed that $CD4^+$ T cell populations (indicated by black staining) in wild type and mutant were predominantly stromal at both days 0.5 and 3.5 p.c. (20x). Sections of wild type and mutant spleens taken from the same mice were tested in parallel as positive control (not shown). Abbr. ge: glandular epithelium; le: luminal epithelium; s: stroma.

Figure 1

A

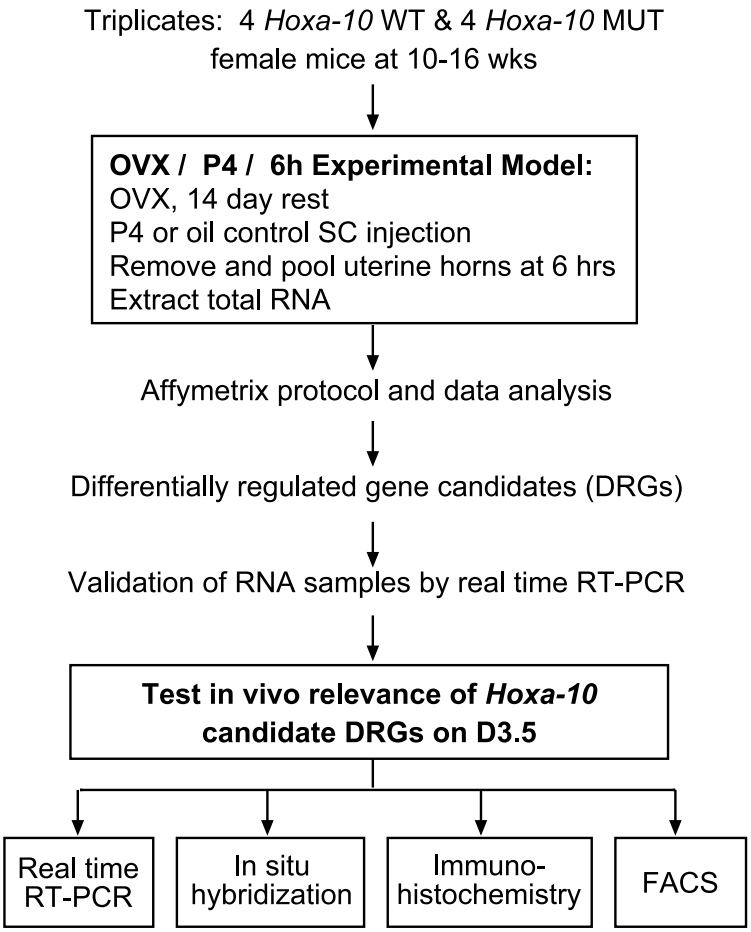
Triplicates: 4 *Hoxa-10* WT & 4 *Hoxa-10* MUT female mice at 10-16 wks
OVX / P4 / 6h Experimental Model:
OVX, 14 day rest
P4 or oil control SC injection
Remove and pool uterine horns at 6 hrs
Extract total RNA
Affymetrix protocol and data analysis
Differentially regulated gene candidates (DRGs)
Validation of RNA samples by real time RT-PCR
Test in vivo relevance of *Hoxa-10* candidate DRGs on D3.5
Real time RT-PCR
In situ hybridization
Immuno-histochemistry
FACS

B

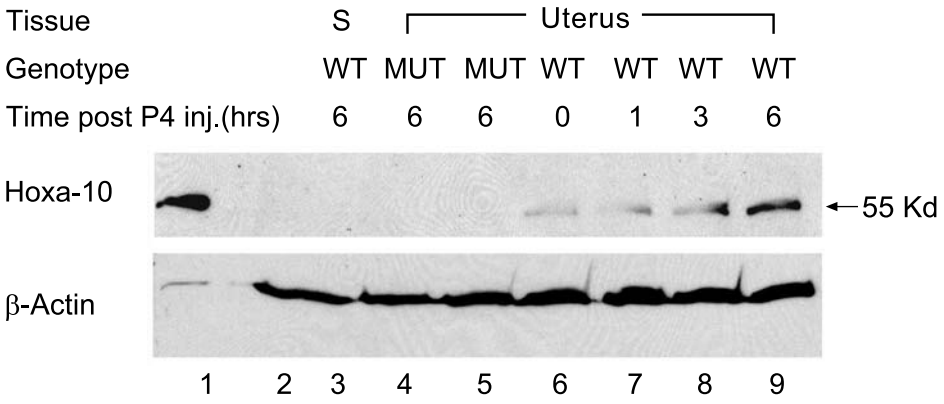
Tissue S Uterus
Genotype WT MUT MUT WT WT WT WT
Time post P4 inj.(hrs) 6 6 6 0 1 3 6
Hoxa-10
55 Kd
β-Actin
1 2 3 4 5 6 7 8 9

Figure 2

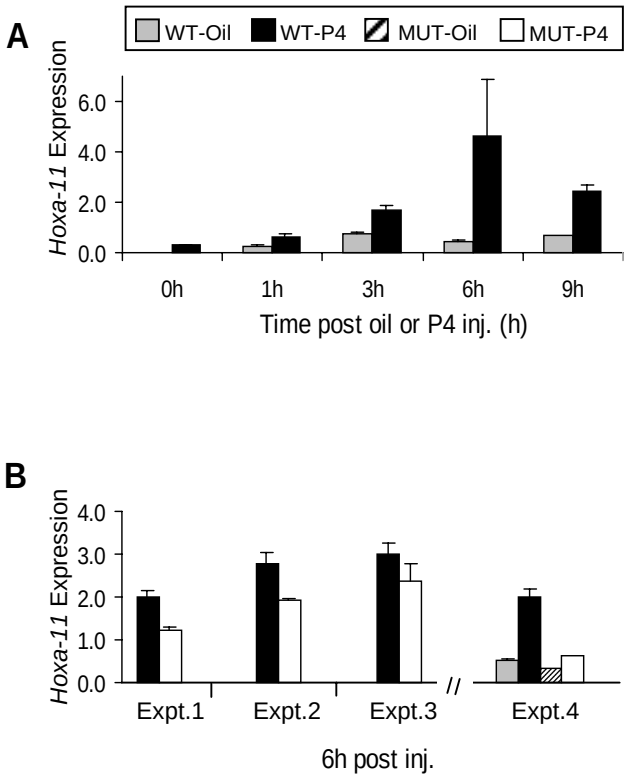
A
WT-Oil
WT-P4
MUT-Oil
MUT-P4
Hoxa-11 Expression
6.0
4.0
2.0
0.0
0h
1h
3h
6h
9h
Time post oil or P4 inj. (h)
B
Hoxa-11 Expression
4.0
3.0
2.0
1.0
0.0
Expt.1
Expt.2
Expt.3
Expt.4
6h post inj.

Figure 3

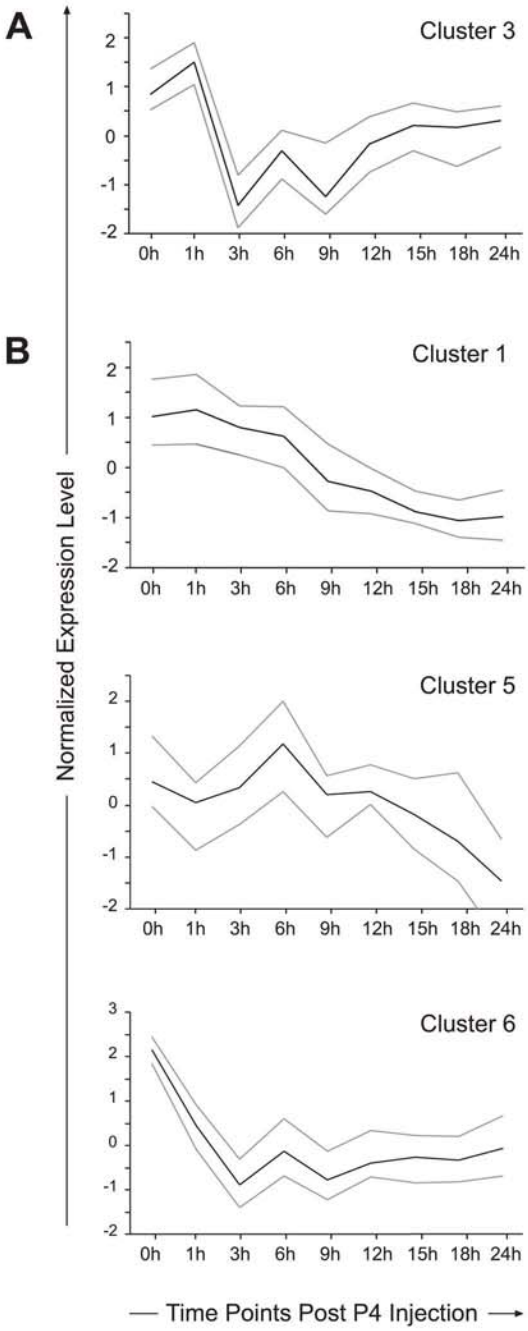

Ig Genes Enriching Cluster 3
40 of the 51 genes (78%) in this cluster were B-lymphocyte specific *Ig* genes.

DRGs Enriching Cluster 1 (N=12)
kallikrein 13
leptin receptor
neighbor of A-kinase anchoring protein 95
neuroblastoma, suppression of tumorigenicity 1
nuclear receptor subfamily 4, group A, member 1
N-myc downstream regulated 2
tenascin X
kruppel-like factor 9
insulin-like growth factor binding protein 3
thioether S-methyltransferase
2 ESTs

DRGs Enriching Cluster 5 (N=7)
adrenomedullin
lipocalin 2
cytochrome P450, 2e1, ethanol inducible
xanthine dehydrogenase
TGFB inducible early growth response
homeo box A11, opposite strand transcript
procollagen, type XV

DRGs Enriching Cluster 6 (N=15)
malic enzyme, supernatant
lactotransferrin
nudix-type motif 3
immunoglobulin heavy chain 3 (serum IgG2b)
claudin 5
ca3
solute carrier family 27, member 1
cadherin 16
stearoyl-coenzyme A desaturase 1*
cyclin-dependent kinase inhibitor 1C (P57)
adipocyte complement related protein of 30kDa
adipsin
2 ESTs

Figure 4

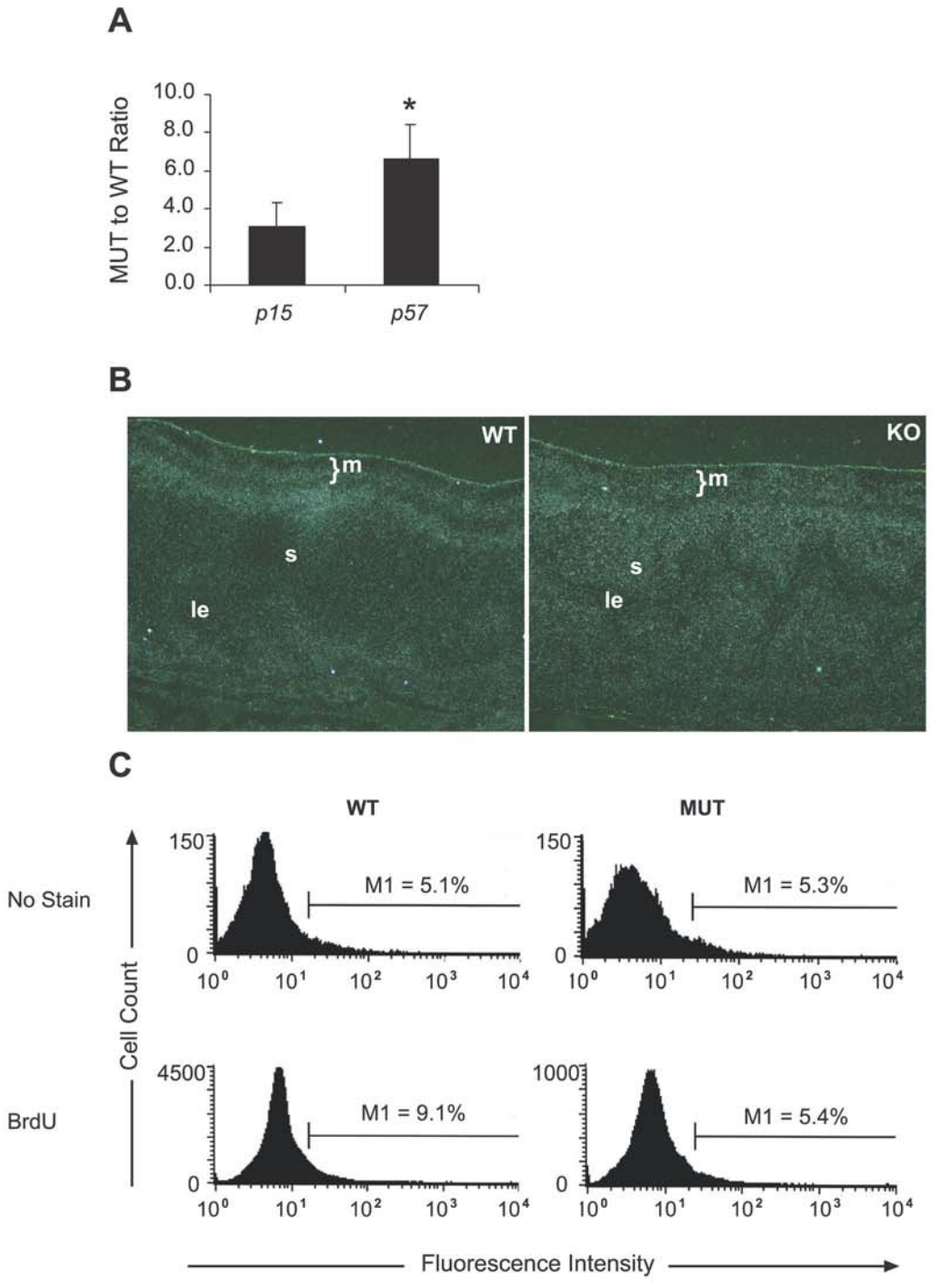
A
MUT to WT Ratio
10.0
8.0
6.0
4.0
2.0
0.0
*
p15
p57
B
WT
KO
}m
s
le
C
WT
MUT
No Stain
BrdU
Cell Count
150
0
M1 = 5.1%
M1 = 5.3%
4500
1000
M1 = 9.1%
M1 = 5.4%
10^0 10^1 10^2 10^3 10^4
Fluorescence Intensity

Figure 5

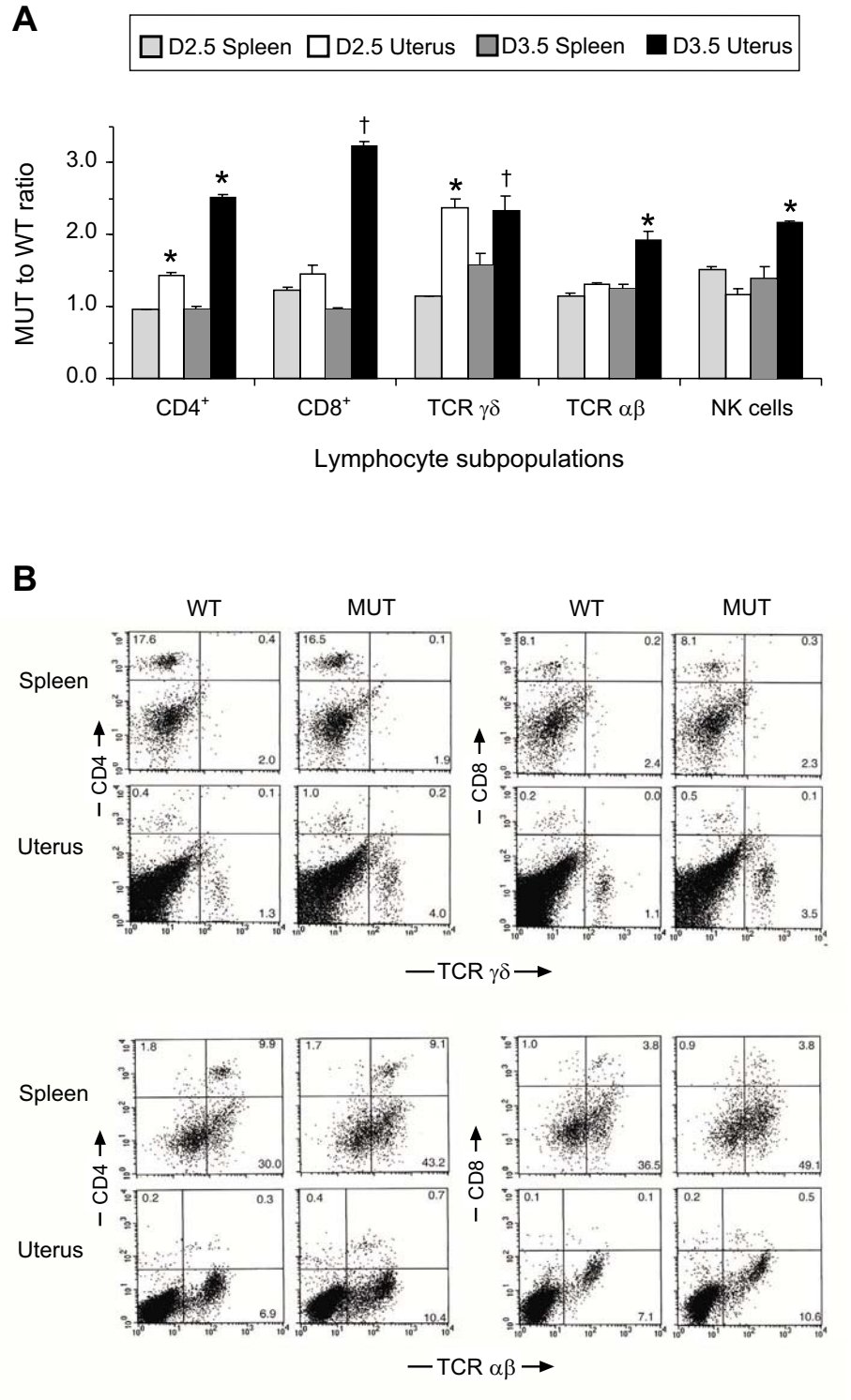
A
D2.5 Spleen
D2.5 Uterus
D3.5 Spleen
D3.5 Uterus
MUT to WT ratio
0.0
1.0
2.0
3.0
CD4+
CD8+
TCR γδ
TCR αβ
NK cells
Lymphocyte subpopulations
B
WT
MUT
WT
MUT
Spleen
Uterus
CD4
CD8
TCR γδ
TCR αβ

Figure 5

C